Polymer 51 (2010) 922–935

Contents lists available at ScienceDirect

Polymer

journal homepage: www.elsevier.com/locate/polymer

Flow induced orientation of multiwalled carbon nanotubes in polycarbonate nanocomposites: Rheology, conductivity and mechanical properties

Samaneh Abbasi [a], Pierre J. Carreau [a,*], Abdessalem Derdouri [b]

[a] CREPEC, Department of Chemical Engineering, Ecole Polytechnique, Montreal, Canada
[b] CREPEC, Industrial Materials Institute, National Research Council Canada, Boucherville, Canada

ARTICLE INFO

Article history:
Received 7 October 2009
Received in revised form
22 December 2009
Accepted 26 December 2009
Available online 11 January 2010

Keywords:
Multiwalled carbon nanotube
Polycarbonate/MWCNT
Percolation

ABSTRACT

We investigated the effect of flow field and deformation rate on the nanotube alignment and on the properties of PC/multiwalled carbon nanotube nanocomposites. Samples of various MWCNT loadings were prepared by diluting a commercial masterbatch containing 15 wt% nanotubes using optimized melt mixing conditions. Different processing conditions were then used to systematically change the degree of nanotube alignment, from random orientation to highly aligned. Morphological studies and Raman spectroscopy analysis revealed that the nanotubes are preferentially aligned in the flow direction, particularly at large injection or compression rates. Rheological measurements corresponding to high shear rate conditions showed drastic changes in the viscoelastic behavior. The complex viscosity significantly decreased and percolation threshold notably rose. High degrees of nanotube alignment also resulted in a significant increase in the electrical percolation threshold. The mechanical properties of the nanocomposites for different nanotube loadings were also shown to depend on the processing conditions, and somehow improved when the material was processed at higher rates. Finally, we used a power-law type equation to correlate the percolation behavior and the nanotube alignment. The estimated percolation threshold and the power index, q, significantly increase with the degree of nanotube alignment as determined by Raman analysis.

1. Introduction

For the last two decades, carbon nanotubes (CNTs) have attracted a strong interest due to their unique electronic structure and extraordinary properties [1]. An extensive research effort has been devoted to the CNTs fabrication, characterization and development of applications. Their intrinsic structure, size scale and aspect ratio suggest a variety of applications in nanoelectronics, sensors and field emission as well as high performance nanocomposites.

Recently, considerable attention has been devoted to carbon nanotube/polymer composites from both processing and application points of view. Besides the individual properties of carbon nanotubes, numerous potential benefits are expected when they are employed as reinforcing agents in polymers. However, the efficiency of nanotubes to live up to their theoretical potential depends on a good dispersion within the host polymer. Three methods are commonly used to incorporate nanotubes into a polymer: solution mixing and film casting of suspensions of nanotubes in dissolved polymers, in situ polymerization of nanotube-polymer monomer mixture and finally mixing of nanotubes in molten polymers. Melt mixing is the industrially preferred method in many cases because of its environmentally benign character, its versatility and its compatibility with current polymer processing techniques.

The intense interest in carbon nanotubes incorporated into polymeric materials stems from their potential to reach thermal, electrical and rheological percolations at relatively small concentrations [2–10]. At the percolation point, the formation of a filler network or interconnecting structure creates additional and large contributions to the nanocomposites properties. For sphere and ellipsoids fillers the percolation behavior is well understood [11], while the onset of percolation in the case of high aspect ratio fillers such as nanotubes strongly depends on their alignment. When the nanotubes are aligned in the polymer matrix the probability of tube–tube contacts decreases and consequently the percolation threshold raises [2,12–14]. Accordingly, the full exploitation of the nanotube properties in polymer composite applications will require an exceptional control of the nanotube alignment in macroscopic parts.

* Corresponding author. Tel.: +1 514 340 4711x4924, fax: +1 514 340 2994.
E-mail address: pcarreau@polymtl.ca (P.J. Carreau).

0032-3861/$ – see front matter © 2010 Elsevier Ltd. All rights reserved.
doi:10.1016/j.polymer.2009.12.041

It is well known that the microstructure of plastic parts is the result of complex changes imposed to the base polymer by the special processing conditions. Typical thermoplastic processing involves pellet melting, plastication, melt flow and pressurization and finally solidification from the molten state, either by crystallization or vitrification. A consequence of such processing methods is the stresses induced by combination of shear and elongational flow field and cooling [15]. The complex thermo-mechanical history imposed on the polymer during processing leads to substantial spatial variations of chain orientation and the formation of a superstructure influenced by the local dynamics of the process. These effects result in anisotropy of the final physical properties particularly if the polymer is filled with solid particles of various shapes (glass or carbon fibers, clay or mica platelets, and carbon nanotubes or nanofibrils, etc.). The use of carbon nanotube based nanocomposites for commercial applications, thus, needs an understanding of how the processing conditions influence the nanotube networks and subsequently the nanocomposites properties.

Although considerable research has been conducted regarding the physical properties of carbon nanotube filled nanocomposites, including mechanical properties, electrical conductivity and rheological properties, only a few investigations have focused on the practical applications of nanocomposites in various industrial fields [13,16–20].

Polycarbonate (PC), a typical amorphous polymer, is an important commercially available engineering thermoplastic for injection molding applications because of its excellent mechanical properties and processability. Recently, carbon nanotubes have been used as special filler to be incorporated into PC for stiffness reinforcement as well as thermal and electrical conductivities enhancement purposes [21–25].

It is the aim of this study to investigate the influence of high shear conditions on the properties of PC/MWCNT nanocomposites with a special focus on the electrical conductivity and structural changes in the nanotube networks. To this end, we systematically studied the percolation behavior as a function of nanotube orientation, varied from random to highly aligned by shearing the nanocomposites through different processing methods.

It is still unclear how to truly and conveniently characterize the nanotube alignment in nanocomposites. Microscopic techniques are widely used to qualitatively determine alignment in the polymer matrix. X-ray diffraction (XRD) is also generally used to ascertain the degree of orientation. The orientation of the crystalline phase is well detected by using the X-ray method; however, DSC and XRD measurements showed that even after long time annealing there was no crystallization induced in the parts. Moreover, more than 50 wt% of MWCNT was required to attain the intensity to detect nanotube alignment [26]. Consequently, we used Laser Raman spectroscopy as an alternative method to quantitatively measure the degree of alignment. Laser Raman analysis is largely used for determining the degree of structural ordering in molecules or the presence of defects in graphitic-like materials. This non-destructive technique also provides information on the microstructure of crystalline materials such as vibration of crystal lattices, electron structure and integrity of the crystal structure, etc. [27]. Polarized Raman spectroscopy was previously used on aligned MWCNTs to show that the observed relative intensities of the Raman *D* and *G* bands are sensitive to the orientation of the nanotubes [28–33]. In polymer nanocomposites, Raman spectroscopy was applied in order to get information of the MWNT orientation, alignment and crystallinity [13,17].

With the aim of finding a correlation between the rheological and electrical properties of the PC/MWCNT nanocomposites, we studied the effect of nanotube alignment on both rheological and electrical conductivity percolation thresholds. Furthermore, we characterized the mechanical properties of the microinjected parts to have an idea on how polymer processing affects the mechanical structure of the nanocomposites. We optimized the nanocomposite preparation using various characterization methods. As nanotubes intertwine into agglomerates that are difficult to disperse we used a polymer/carbon nanotube masterbatch and diluted it to the required concentrations by adding the neat polycarbonate. This insured consistent and reproducible results.

2. Experimental

2.1. Materials

A masterbatch of 15 wt% MWCNT in PC was purchased from Hyperion Catalysis International, Cambridge, MA. According to the supplier, the carbon nanotubes are vapor grown and typically consist of 8–15 graphite layers wrapped around a hollow 5 nm core [10]. The diameter range was stated to vary from 15 to 50 nm and the length range of 1–10 μm as was confirmed by TEM characterization. The masterbatch was diluted with a polycarbonate (Calibre 1080) supplied by Dow Chemical to prepare nanocomposite samples of various loadings. This PC is not necessarily the same as the polycarbonate found in the masterbatch. Considering the small quantity of masterbatch used to prepare the nanocomposites, the original PC of the masterbatch is only a small fraction of the nanocomposites and does not significantly affect the results.

2.2. Nanocomposite preparation and molding

The composites were produced by melt mixing the masterbatch with the neat PC. Prior to mixing, all materials were dried for a minimum of 4 h at 120 °C under vacuum. Eight different composites with MWCNT contents between 0.5 and 15 wt% MWCNT were prepared using a 18 mm diameter twin-screw extruder, Leistritz ZSE 18HP, operating at 100 rpm and 210 °C. Compression molding, conventional injection molding, micro-injection molding and microinjection-compression molding were then employed to apply different levels of shear or deformation rate on the nanocomposites. Prior to each processing, the materials were dried under the conditions previously mentioned. Compression molding of dried nanocomposites were done using a Carver laboratory press, model 3912, operated manually at 270 °C. The disk shaped molded samples of 60 mm diameter and 1.5 mm thickness were then cooled down to room temperature. For the conventional injection molding we used a Sumitomo SE50S electrical 50 ton injection molding machine to mold standard dog-bone shaped tensile test specimens of 150 mm in total length, with a gage section 10 mm wide by 4 mm thick by 80 mm long. Injection was done at an average barrel temperature of 300 °C under a pressure of approximately 100 MPa while injection speed was constant at 400 mm/s. The mold temperature was kept constant at 80 °C and cooling time was set to 10 s. Micro-injection molding was done using a Battenfeld Microsystem 50 micromolding machine operating at the same processing conditions as the conventional one. To investigate the effect of mold geometry, two different mold cavities were used: one having a dog-bone shape of 15 mm long, with the center section of 1 mm wide by 0.78 mm thick by 4.3 mm long, gated at one end, and the other a disk shape of 25 mm in diameter and 1 mm thick, gated at the center. To examine the effect of the injection speed two additional injection speeds were also used in the case of the dog-bone samples: 200 and 800 mm/s. Finally, micro-injection-compression molding was employed to evaluate the effect of applying a compression step at the end of the injection phase on the part properties, using the centrally gated disk cavity

with the same dimensions as described before. The process consisted of injecting the melt into the cavity, while the mold was not totally closed. This leads to an initial cavity filling under a lower pressure than if the mold was closed, as in conventional injection molding. After the injection stage, the mold was closed to compress the melt and to completely fill the cavity. The operating conditions in this case are the same as micro-injection molding using only 400 mm/s for the injection speed. The gap between the mold plates was about 1.2 mm and the mold closing speed used in this experiment was 1.5 mm/s.

2.3. Morphological characterization

The morphology of nanocomposites was studied through scanning and transmission electron microscopy (SEM and TEM) and atomic force microscopy (AFM). For SEM we used a high resolution Hitachi S-4700 microscope while for AFM we utilized a multimode Veeco scanning probe in tapping mode. Both SEM and AFM were done on ultramicrotomed surfaces of samples that were cut with a diamond knife at room temperature. SEM samples were coated with a vapor deposit of platinum for 25 s. TEM was done on ultrathin sections of nanocomposites using a Hitachi HD-2000 microscope. For injection molded samples, the specimens were cut both parallel and perpendicular to the flow direction.

2.4. Raman spectroscopy

Raman spectra were collected using a Renishaw spectrometer equipped with an in Via Raman microscope fitted with a 20 × objective. The samples were excited using a NIR laser (785 nm) with a grating of 1200 g/mm in a regular mode. Measurements were carried out at two different orientations of the polarized laser beam with respect to the flow direction in the samples (Fig. 1). In the first configuration (Fig. 1a), the flow direction was parallel (0°) to the direction of the polarized beam; in the second one (Fig. 1b), it was perpendicular (90°). The MWCNT alignment in the composite was determined by comparing the spectra for parallel and perpendicular directions.

2.5. Rheological measurements

All the rheological measurements were carried out using a stress-controlled rheometer (CSM rheometer of Bohlin Instruments) equipped with a 25 mm parallel plate geometry under nitrogen atmosphere. Prior to measurements, the samples were dried for a minimum of 4 h at 120 °C. To investigate the viscoelastic properties of the nanocomposites after processing, molded disks by compression, micro-injection-compression and micro-injection were used. They were put in the rheometer with precaution to avoid the formation of any bubbles or surface defects. Small amplitude oscillatory shear (SAOS) tests were carried out between 0.06 and 200 rad/s in the linear viscoelastic regime. This regime was established in the standard way by measuring the modulus at constant frequency (10 rad/s) and increasing strain magnitude. Further, long-time measurements (up to 3 h) were conducted to investigate the thermal stability of the nanocomposite samples. We assumed that the particle sizes were sufficiently small compared to the gap; however, the absence of apparent slip at the wall has been ascertained by varying the gap from 0.5 to 1.5 mm. The differences were found to be insignificant, less than the reproducibility of the data estimated to be within 3.5% for all the frequency sweep tests conducted with the various nanotube loadings.

In addition, the effect of high shear on the microstructure of the nanocomposites was evaluated by subjecting each sample to a high shear stress for various periods of time at 300 °C (injection temperature). SAOS measurements were then performed without any rest time between the preconditioning step and the SAOS test.

Finally a capillary rheometer (Rosand) with a capillary of 32 mm length and 1 mm diameter was used to determine the steady-state viscosity as a function of shear rate for the neat polymer and nanocomposites.

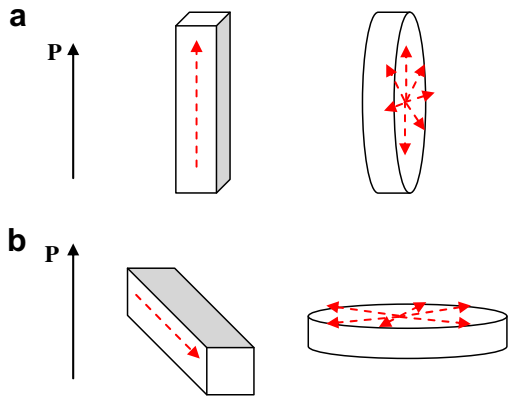

Fig. 1. Schematic for Raman spectroscopy. Characteristic scattering configurations for the Raman spectroscopic measurements: (a) Parallel position of specimen, corresponding to 0° angle between polarization direction (P) and flow direction (dashed arrow); (b) Perpendicular position of specimen, corresponding to 90° angle between polarization direction (P) and flow direction (dashed arrow).

2.6. Electrical conductivity measurements

The volume resistivity of the PC/MWCNT nanocomposite samples was determined by measuring the DC resistance across the thickness of compression molded disks using a Keithley electrometer model 6517 equipped with a two probe test fixture. This equipment allows resistance measurements up to 10^{17} Ω. The level of applied voltage, adapted to the expected resistance, was in the range of 1000 V for the neat PC and samples containing up to 1 wt% MWCNT and 100 V for samples with 2 wt% and more MWCNT. However, since for the more conductive samples, the accuracy of this equipment failed, samples with more than 2 wt% MWCNT, were tested using the more adequate Keithley electrometer model 6220 connected to a current source (Aligent 34 401 A, 6½ Digit Multimeter). This electrometer can be used only for semi-conductive materials. For each sample the *I–V* curve was obtained and the sample resistance was determined from the slope of the curve. The resistance was then converted to volume resistivity, ρ_v, using the formula

$$\rho_v = AR_v/D \quad (1)$$

where A is the contact surface area, D is the thickness of the sample, and R_v is the measured resistance. The electrical conductivity (σ) of the nanocomposites is the inverse of volume resistivity. Prior to measurements all samples were dried for a minimum of 4 h at 120 °C.

2.7. Mechanical properties

An Instron Micro Tester model 5548 was used to measure the tensile strength, modulus and elongation at break of nanocomposites using microinjected tensile bars having a gage length of 4.3 mm. The tests were performed at room temperature using a crosshead speed of 50 mm/min, based on ASTM D638, and data acquisition rate of 13 points per second. The tensile strength and elongation at break could be directly obtained from the stress–strain

curves. To obtain the elastic modulus, a linear regression technique was utilized to define the slope of the stress–strain curve in the initial region before yield. All the reported values were calculated as average over six specimens for each composition and each condition with a maximum deviation of ±8%.

3. Effective shear rate estimation

Polymer processing proceeds generally under a complex flow field, which is a combination of elongational and shear flows. Injection molding is one of the most complex non-isothermal processes with a combination of different flow fields. The conditions are more complex in the case of micro-injection molding particularly micro-injection of disk shaped samples where the effect of elongational flow is more pronounced. Another complexity arises from the behavior of polymer melts at the relatively high deformation rate of these processes and at different planes from the surface to the core of the sample. Since the accurate modeling of the processes is not the main idea of this study we made some simple assumptions to estimate the effective shear rates encountered in the processes used in this work. Although the elongational flow could play an important role and affect the nanotubes alignment and polymer chains orientation especially for viscoelastic materials, the following estimates are based on the assumption that for these flows the fluid is purely viscous.

The flow geometries in compression molding, conventional injection molding, micro-injection molding and micro-injection-compression molding are illustrated in Fig. 2. In principle, these problems should be solved using non-isothermal viscoelastic models, but this would result in rather complicated numerical techniques using sophisticated software packages. Useful approximations, however, are obtained by considering isothermal Newtonian or power-law models and assuming the same orientation profile from the surface to the core of the samples.

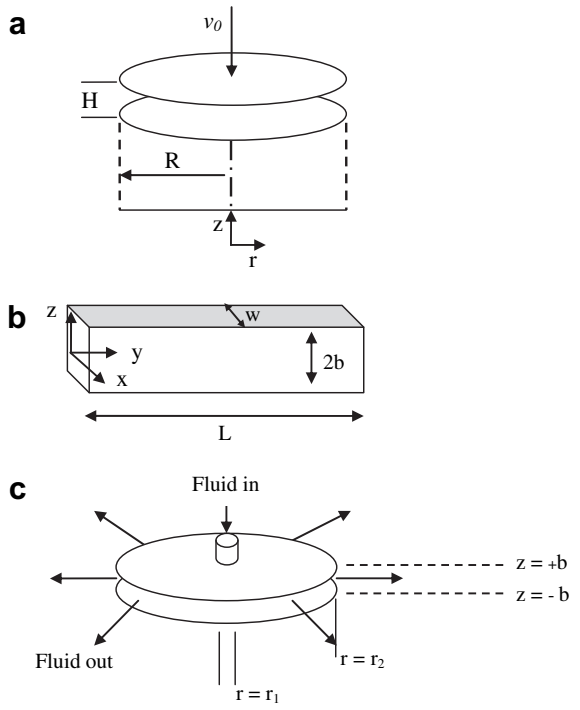

Fig. 2. (a) Squeezing flow in compression molding between two parallel disks (b) longitudinal flow of conventional and micro-injection molding of tensile bar (c) radial flow of micro-injection molding of disk shaped sample.

The calculations are provided for the 5 wt% MWCNT/PC nanocomposites that obey the following expression:

$$\eta = m|\dot{\gamma}|^{n-1} + \eta_\infty \tag{2}$$

where m and n are the power-law parameters and η_∞ is the limiting viscosity at high shear rate. This expression contains two terms: the first term is a power-law viscosity and the second term is a Newtonian viscosity. At low shear rate the viscosity obeys a power-law behavior whereas at high shear rate the viscosity tends towards a constant value.

In a recent article, Abbasi et al. [34] investigated the effect of pre-shearing on the viscoelastic properties of PC/MWCNT nanocomposite samples, at high and low stresses. They pointed out that a high degree of nanotube alignment is obtained when high nanotube loadings are used. Due to the nanotubes alignment, the Cox-Merz rule could not be applied to the dynamic viscosity measurements to determine the power-law parameters of Eq. (2). Steady shear viscosity measurements were therefore carried out for various nanotube loadings at 300 °C (injection temperature) using the capillary rheometer and the results are shown in Fig. 3. As observed for the complex viscosity data reported in ref. [34], the viscosity increases markedly with nanotube loading and the suspensions become more shear-thinning. However, the shear viscosity values of Fig. 3 are considerably smaller than those reported in ref. [34] due to nanotube alignment in shear flow as shown below. The 5 wt% nanocomposite data was fitted using the power-law equation above, resulting in the following parameters values: $m = 3.77 \times 10^3$ Pa s^n, $n = 0.34$ and $\eta_\infty = 40$ Pa s. The fit is shown to be excellent.

3.1. Compression molding

In compression molding (Fig. 2a) a blank of polymeric material is assumed to fill completely the region between two circular parts of the disk shaped mold of radius R and it can only flow on squeezing along the r direction. The bottom disk is fixed and the upper disk is made to approach the lower one very slowly with a constant speed of v_0 starting from an initial height of H. A simple form of the velocity profile for this problem is given by [35]:

$$v_r = \frac{1}{2\eta_e}\left(\frac{dp}{dr}\right) z(z - H) \tag{3}$$

where η_e is the effective viscosity. The pressure profile is as follows:

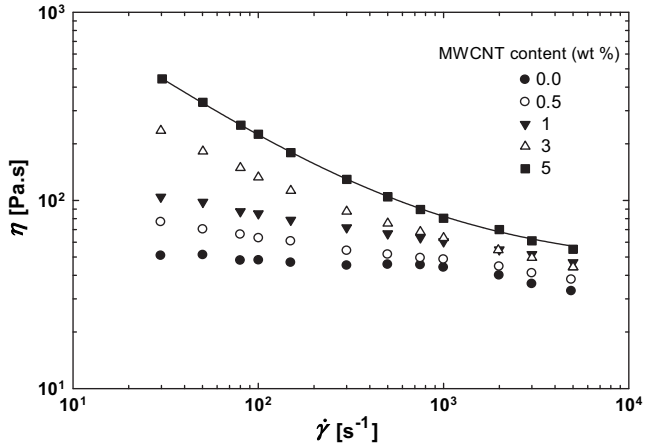

Fig. 3. Viscosity versus shear rate for PC/MWCNT nanocomposites at 300 °C. The line shows the best fit using Eq. (2).

$$p = p_{atm} + \frac{3\eta_e v_0 R^2}{H^3}\left[1 - \left(\frac{r}{R}\right)^2\right] \quad (4)$$

The effective rate of deformation can be calculated from the velocity profile:

$$\dot{\gamma} = \sqrt{2\left(\frac{\partial v_r}{\partial r}\right)^2 + 2\left(\frac{v_r}{r}\right)^2 + \frac{1}{2}\left(\frac{\partial v_r}{\partial z}\right)^2} \quad (5)$$

Combining Eqs. 3–5, the following expression for the effective rate of deformation is obtained:

$$\dot{\gamma} = \frac{3v_0}{H^3}\sqrt{4z^2(z-H)^2 + \frac{r^2}{2}(2z-H)^2} \quad (6)$$

For a power-law fluid the velocity profile is as follows [36]:

$$v_r = \frac{H^{1+1/n}}{1+1/n}\left(-\frac{1}{mr^n}\frac{dp}{dr}\right)^{1/n}\left[1 - \left(\frac{z}{H}\right)^{1+1/n}\right] r \quad (7)$$

with the pressure profile as:

$$p = p_{atm} + \frac{v_0^n}{H^{2n+1}}\left(\frac{2n+1}{2n}\right)^n\left(\frac{mR^{n+1}}{n+1}\right)\left[1 - \left(\frac{r}{R}\right)^{n+1}\right] \quad (8)$$

The effective rate of deformation can then be obtained using Eq. (5).

The press can operate at speeds between 4 and 34 mm/s. Assuming $H = 1.5$ mm and $R = 15$ mm, the $\dot{\gamma}_e$ values at $z = H/4$ and $r = R/2$ as a typical point is obtained for the whole range of operating velocity (Table 1).

3.2. Injection molding

3.2.1. Conventional injection and micro-injection molding of tensile bar

We consider the flow of polymer melt into thin rectangular cavities as illustrated in Fig. 2b. The velocity profile for a Newtonian fluid is [37]:

$$v_y = \frac{b^2\Delta p}{2l\eta_e}\left[1 - \left(\frac{z}{b}\right)^2\right] \quad (9)$$

where Δp is the pressure difference between p_0, the pressure at $y = 0$ or injection pressure, and p_{atm}. The shear rate is obtained from the velocity profile as follow:

$$\dot{\gamma} = \left|\frac{\partial v_y}{\partial z}\right| \quad (10)$$

The effective shear rate is then calculated using the following equation for a Newtonian fluid of η_e:

$$\dot{\gamma}_e = \frac{\Delta p}{l\eta_e} z \quad (11)$$

For a power-law fluid the effective shear rate can be obtained from the following equation:

$$\dot{\gamma}_e = \left|\left(\frac{\Delta p}{ml} z\right)^{1/n}\right| \quad (12)$$

For the conventional injection molding case, we use $p_0 = 100$ MPa, $b = 2$ mm and $L = 80$ mm to calculate the effective shear rate at $l = L/2$ and $z = b/4$ for the 5 wt% MWCNT/PC nanocomposites. For micro-injection molding, an estimated effective shear rate can be obtained taking $p_0 = 100$ MPa, $b = 0.39$ mm and $L = 4.3$ mm, $l = L/2$ and $z = b/4$. The values are reported in Table 1.

3.2.2. Microinjection and micro-injection-compression molding of disk

The radial flow of the polymeric melt between two disks is considered in this section (Fig. 2c). For a Newtonian melt, the velocity profile in this case is as follows [35,37]:

$$v_r = \frac{\Delta p b^2}{2\eta_e r \ln(r_2/r_1)}\left[1 - \left(\frac{z}{b}\right)^2\right] \quad (13)$$

Using Eq. (5), the effective shear rate is estimated from the following equation:

$$\dot{\gamma}_e = \frac{\Delta p b^2}{2\eta_e r \ln(r_2/r_1)}\sqrt{\frac{2}{r^2}\left[1 - \left(\frac{z}{b}\right)^2\right]^2 + \frac{2}{b^2}\left(\frac{z}{b}\right)^2} \quad (14)$$

For a power-law fluid there is no analytical solution for this case. Neglecting the contribution of the elongational component of the flow, the following simplified expression is obtained [38]:

$$v_r = \frac{1}{r}\left(\frac{n}{n+1}\right)\left[\frac{(1-n)\Delta p}{(r_2^{1-n} - r_1^{1-n})}\frac{b^{n+1}}{m}\right]^{1/n}\left[1 - \left(\frac{z}{b}\right)^{(n+1)/n}\right] \quad (15)$$

The effective shear rate is then obtained using Eq. (5). For $p_0 = 100$ MPa, $2b = 1$ mm, $r_1 = 0.75$ mm and $r_2 = 12.5$ mm the $\dot{\gamma}_e$ values of micro-injection molding of disk at $z = b/2$ and $r = (r_2 - r_1)/2$ are reported in Table 1.

In micro-injection-compression, each phase (injection and compression phases) features a specific shear rate. However, the applied shear rate in the second phase (compression) is almost negligible due to very low closing speed. The effective shear rate in injection phase can be calculated using Eqs. (13) and (14). The only difference with micro-injection of the disk is the injection pressure that is about 15 MPa in this case. The $\dot{\gamma}_e$ values at $z = b/2$ and $r = (r_2 - r_1)/2$ of the disk are then obtained (Table 1).

We note that the effective rate calculated for the different processes varies from a very low value of 1.8 s^{-1} for compression molding to 1.8×10^9 s^{-1} for micro-injection of dog-bone samples. However, the values of $\dot{\gamma}_e$ calculated for the last three injection processes using the power-law expression are way excessive. Referring to Fig. 3, the shear viscosity of the 5 wt% nanocomposite reaches the high shear plateau, η_∞, for $\dot{\gamma} \approx 10^4$ s^{-1}. Hence, the

Table 1
Effective shear rates encountered in the processes and Raman intensity ratios parallel/perpendicular to the flow direction.

	Effective shear rate $\dot{\gamma}_e$ (s^{-1})		Raman intensity ratio parallel/perpendicular		
	Newtonian model	Power-law model	$D_\Pi/D_\perp$	$G_\Pi/G_\perp$	$(D/G)_\Pi/(D/G)_\perp$
Compression molding (disk)	14.5–122	1.8–20	1.03	1	1.03
Micro-injection-compression molding (disk)	4×10^3	1.2×10^5	1.33	1.2	1.08
Micro-injection molding (disk)	2.7×10^4	3.2×10^7	1.52	1.37	1.1
Conventional injection molding (dog-bone)	3.1×10^4	2.6×10^7	1.71	1.55	1.1
Micro-injection molding (dog-bone)	1.1×10^5	1.8×10^9	1.95	1.75	1.11

calculations based on the Newtonian model with $\eta_e = \eta_\infty = 40$ Pa s are more reasonable except possibly for the compression molding for which the shear rate is more in the power-range. The Raman intensity values of Table 1 are discussed below in light of the effective shear rate.

4. Experimental results

4.1. Morphology

SEM micrographs, taken at the surface of a compression molded sample (the part produced under the lowest shear rate) and a microinjected sample (the part produced under the highest shear rate), are shown in Fig. 4 for 5 wt% nanocomposites.

It can be seen that there is no preferred orientation within the nanocomposite in the compression molded sample (Fig. 4a). However, in the microinjected sample (Fig. 4b), only the ends of the nanotubes, as bright spots, can be observed in the micrographs. Since the injected specimens in this case were cut perpendicularly to the flow direction, seeing only the end of the nanotubes is an indication that the nanotube orientation is in the shear flow direction.

The nanotube orientation can be seen more clearly in AFM micrographs. For the compression molded sample (Fig. 5a) segments of length of some nanotubes can be observed in the phase mode image, while for the microinjected sample (Fig. 5b), cut perpendicularly to the flow direction, only black spots, representing the nanotube ends, are seen. The SEM and AFM micrographs show not only differences in orientation of the nanotubes between the samples made by the two molding processes, but they also indicate that their dispersion within the PC matrix is quite good, particularly in the case of the microinjected samples. The drastically high deformation rates encountered in micro-injection molding contribute strongly not only to the nanotubes alignment but also to their distribution within the polymer matrix. The nanotubes diameter derived from the scale of the AFM micrographs is about 15 nm, remarkably within the range of the information given by the masterbatch supplier, indicating that the nanotubes are most probably individually dispersed.

To help understand more the effect of the shear flow on the nanotube alignment, TEM micrographs of samples prepared using different processing methods are shown in Fig. 6. In the case of the injected samples, the images were all taken from thin sections cut along the flow direction. For the compression molded sample (Fig. 6a) the micrograph does not indicate any preferential orientation. On the other hand, the nanotubes are somehow oriented in the case of the micro-injection-compression molded samples (Fig. 6b); however, it is still far from a perfect orientation and we can see isotropy in the system. Fig. 6c shows the micrograph of a sample prepared by conventional injection molding; a clear orientation of the nanotubes along the length axis can be seen. The highest degree of orientation is obtained for micro-injection molding where the nanotubes are well aligned and most of them are perfectly stretched along their length axis (Fig. 6d). Considering

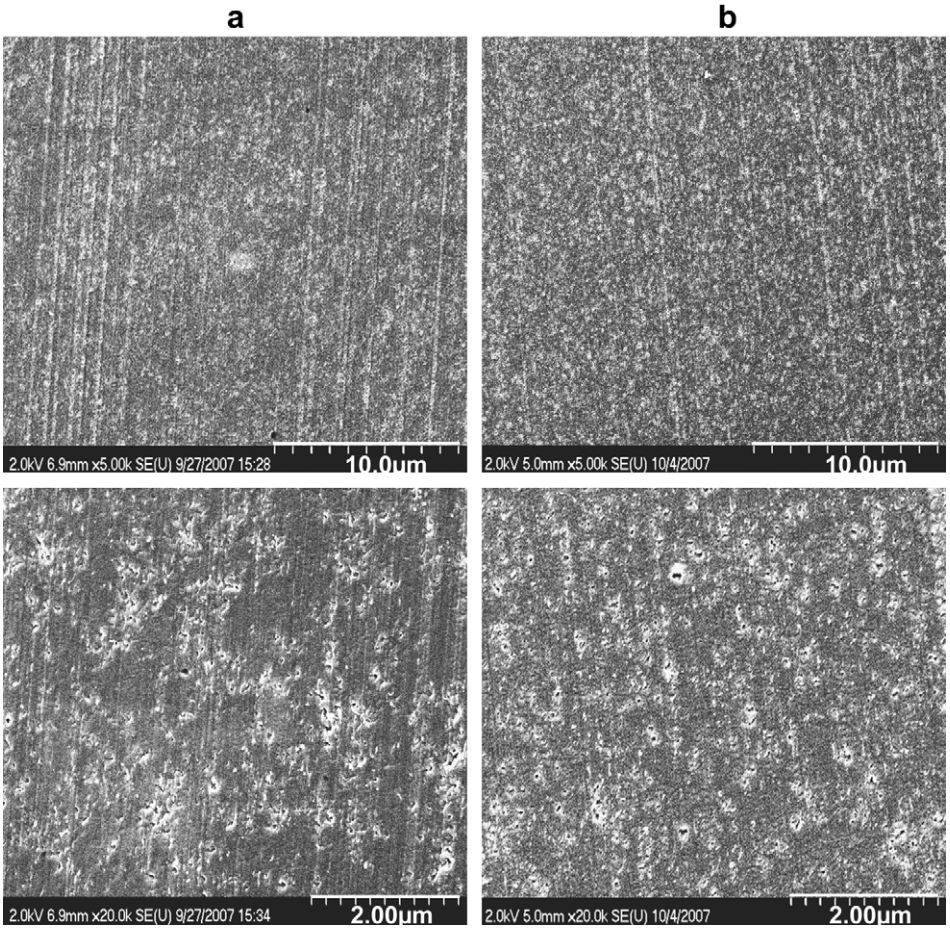

Fig. 4. SEM micrographs of crayon surfaces of PC/5 wt% MWCNT nanocomposites processed in (a) compression molding and (b) micro-injection molding. The top and the bottom micrographs are related to the low and high magnification, respectively.

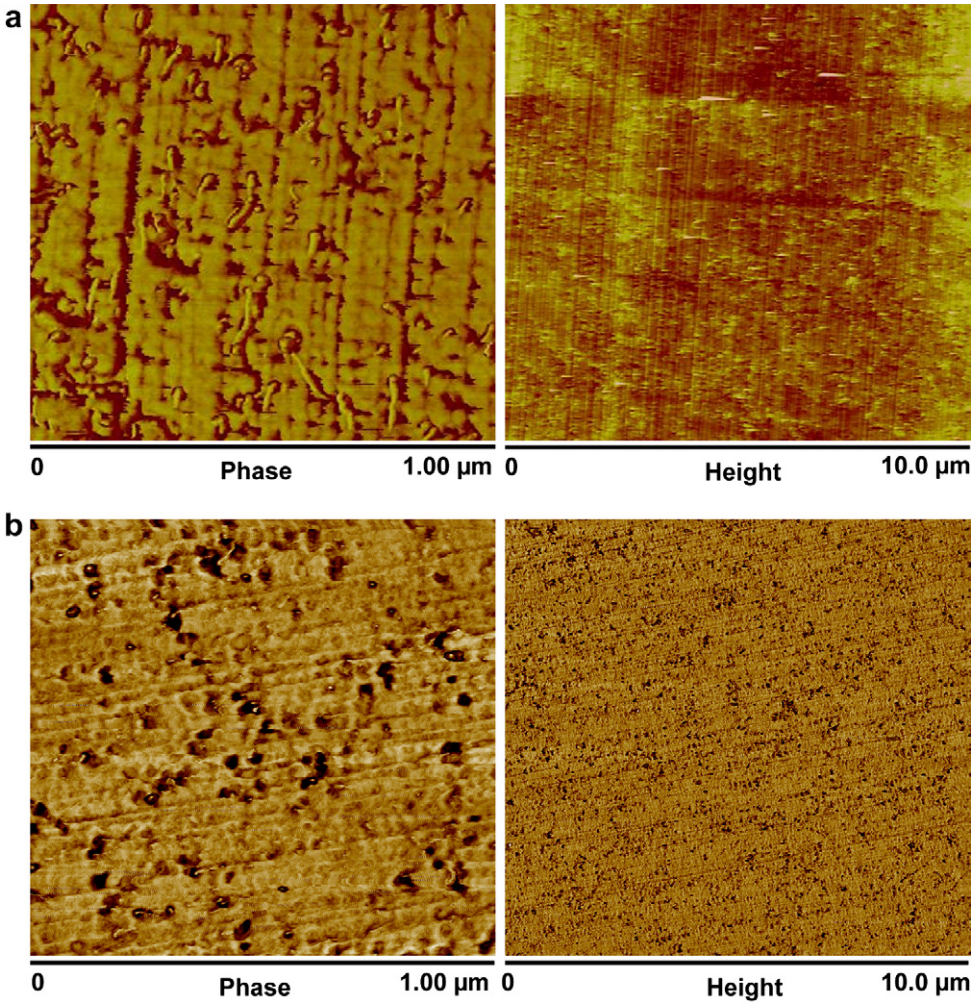

Fig. 5. AFM micrographs of crayon surfaces of PC/5 wt% MWCNT nanocomposites processed in (a) compression molding and (b) micro-injection molding. The left and the right micrographs are related to the phase and height modes, respectively.

the fact that the nanotubes are often strongly entangled, a few nanotubes remain oriented transversely (perpendicular to the flow direction) after injection.

The histograms of the nanotube length distribution are reported in Fig. 7a–d. By nanotube length we mean the end-to-end distance of each segment of nanotube as it can be observed in the micrographs. Since the samples shown in Fig. 6 were cut along the flow direction using a very sharp diamond knife, most nanotubes that are randomly located in the samples are sectioned. However, well flow-oriented nanotubes were parallel to the cutting direction and therefore a large part of their full length is observed in the micrographs. For compression molded samples (Fig. 7a) most of the nanotubes have lengths less than 100 nm. For compression microinjected samples (Fig. 7b) the observed nanotube length is longer and there are some exceeding 200 nm. For conventional injection (Fig. 7c) most of the nanotubes have lengths in the range of 200–400 nm and in the case of micro-injection molding (Fig. 7d) the nanotubes length is in the range of 200–500 nm and in some cases reaches 700 nm. Although these values are still well below the initial length of nanotubes (1–10 μm, as specified in the material section) these values are a good indication of a high degree of nanotube alignment in microinjected parts.

4.2. Raman spectroscopy

Raman spectroscopy was used to further investigate the MWCNT alignment within the polycarbonate matrix. This is a non-destructive spectroscopy technique, which relies on the inelastic scattering of infrared light by molecules upon returning to their lower energy level after excitation. Depending on the frequency of the light used, Raman bands with different intensities are produced by vibration of various active groups within the polymer chains. The vibrational characteristics of these groups can then be used to determine and identify the polymer structure [28]. Carbon nanotubes show resonance-enhanced Raman scattering effects when a visible or near infrared laser is used as the excitation source. Both single walled carbon nanotubes (SWCNTs) and MWCNTs feature bands located in the higher wavenumber region over 500 cm^{-1}; however, Raman bands appearing in the low wavenumber region between 100 and 400 cm^{-1} (known as radial breathing modes or RBM) are a unique characteristic of SWCNTs [29] and are not generally observed for MWCNTs. The Raman spectra of the as-extruded neat polycarbonate and 5 wt% PC/MWCNT nanocomposites are shown in Fig. 8. As it can be observed, the most important Raman bands of polycarbonate are located in the range of 500–1800 cm^{-1} as assigned by Lee et al. [30]. Contrary to carbon

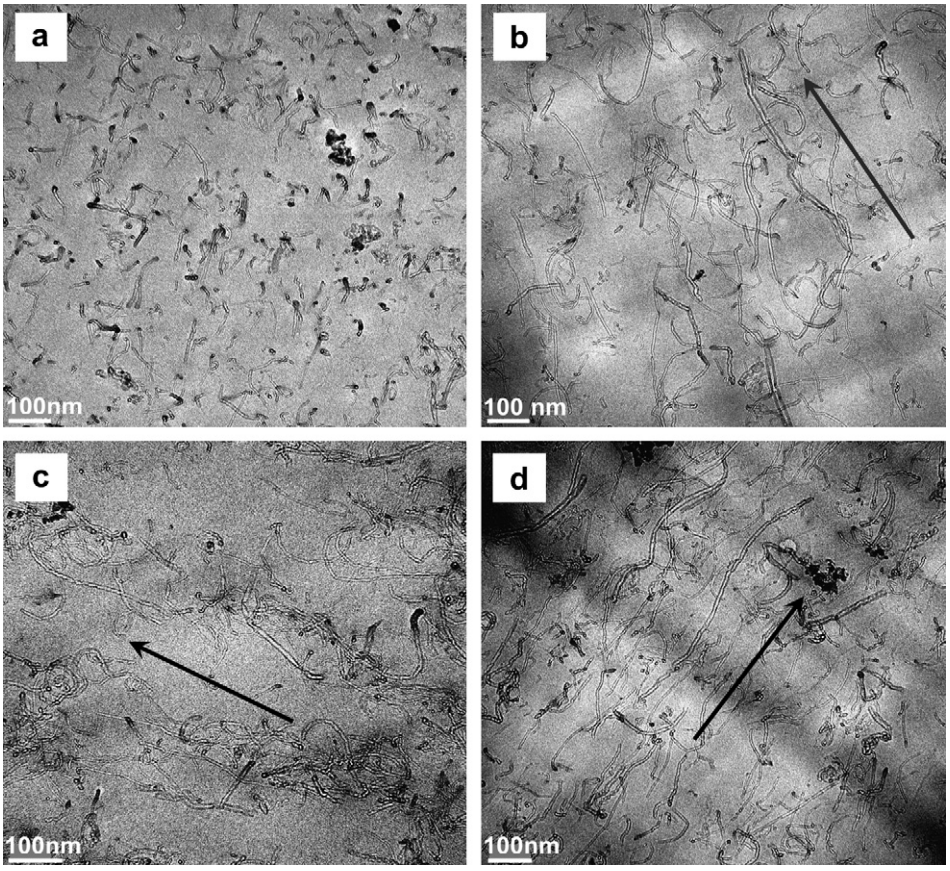

Fig. 6. TEM micrographs of thin sections of PC/5 wt% MWCNT nanocomposites prepared along the flow direction. Samples were (a) compression molded, (b) micro-injection-compression molded (c) conventional injection molded (d) micro-injection molded. Arrows indicate the flow direction.

nanotubes, most polymers including polycarbonate do not show a resonance enhancement effect [27]. In fact, the large differences between the intensity of the nanotube peaks and those arising from a polymeric matrix make the Raman spectroscopy an ideal technique for the study of nanotubes orientation.

As Fig. 8 shows clearly, the Raman bands of polycarbonate almost vanish by incorporation of nanotubes into the matrix. Two important features in the Raman spectrum of MWCNTs are the *D* band (disorder band), located between 1330 and 1360 cm^{-1} and the *G* band (graphite band or TM-tangential mode) located around 1580 cm^{-1}. These bands are clearly observed in the spectrum of PC/MWCNT of Fig. 8. The *D* band originates from the sp^2 hybridized (graphite-like carbon atoms) disorder in the graphitic structure, and is the most sensitive Raman peak to the nanotube alignment. The *G* band, assigned to the in-plane vibration of the graphitic wall, is less sensitive to orientation [31]. Another Raman band in the spectrum of carbon nanotubes, named *G'*, is located at ~2700 cm^{-1} and is also not sensitive to the nanotube alignment [32].

The intensity ratios $D_{\prod}/D_{\perp}$ and $G_{\prod}/G_{\perp}$ parallel/perpendicular to the flow direction were used to assess the degree of nanotube alignment. Raman spectra of PC/5 wt% MWCNT are shown in Fig. 9 for compression molded samples or samples produced under the lowest shear or deformation rate (Fig. 9a and b) and dog-bone shaped microinjected samples or the samples produced under the highest shear rate (Fig. 9c and d).

For the compression molded samples, parallel (Fig. 9b) and perpendicular (Fig. 9a) spectra are almost the same and there are no significant differences between the intensities of the peaks. The $D_{\prod}/D_{\perp}$ and $G_{\prod}/G_{\perp}$ parallel/perpendicular intensity values are therefore close to unity indicating that there is no preferential nanotube alignment in the polycarbonate matrix [10,39]. For microinjected samples, however, there are significant differences between the parallel (Fig. 9d) and perpendicular (Fig. 9c) Raman spectra. The intensities of both bands, *D* and *G*, are much larger in the parallel spectra.

The results obtained from the Raman spectra of the nanocomposites prepared under various levels of deformation rate (i.e. for different polymer processing conditions) are summarized in Table 1. From top to bottom, both ratios increase, demonstrating that the lowest nanotube alignment is found in the compression molded samples and the highest one in the dog-bone shaped microinjected samples. These results are completely in agreement with the morphological analysis and clearly show that the different levels of shear rate applied to the nanocomposites result in significant differences in the nanotube alignment (Table 1). It is shown that when using micro-injection molding, the applied shear rate is much larger than in conventional injection molding (Table 1), for the same injection speed and cavity shape. Therefore, nanotubes are well aligned in the longitudinal flow field of the micro-injection mold of dog-bone shaped (tensile bar) and consequently the highest intensity ratios for both *D* and *G* bands are achieved in this case. In conventional injection molding, the lower level of shear rate results in a lower nanotube alignment even in the longitudinal flow field of the dog-bone shaped cavity and, accordingly, lower intensity ratios of Raman *D* and *G* bands are obtained. On the other hand, the nanotubes alignment decreases noticeably in the case of radial flow of the disk shaped cavity with respect to the longitudinal flow of the tensile bar cavity. Although the applied

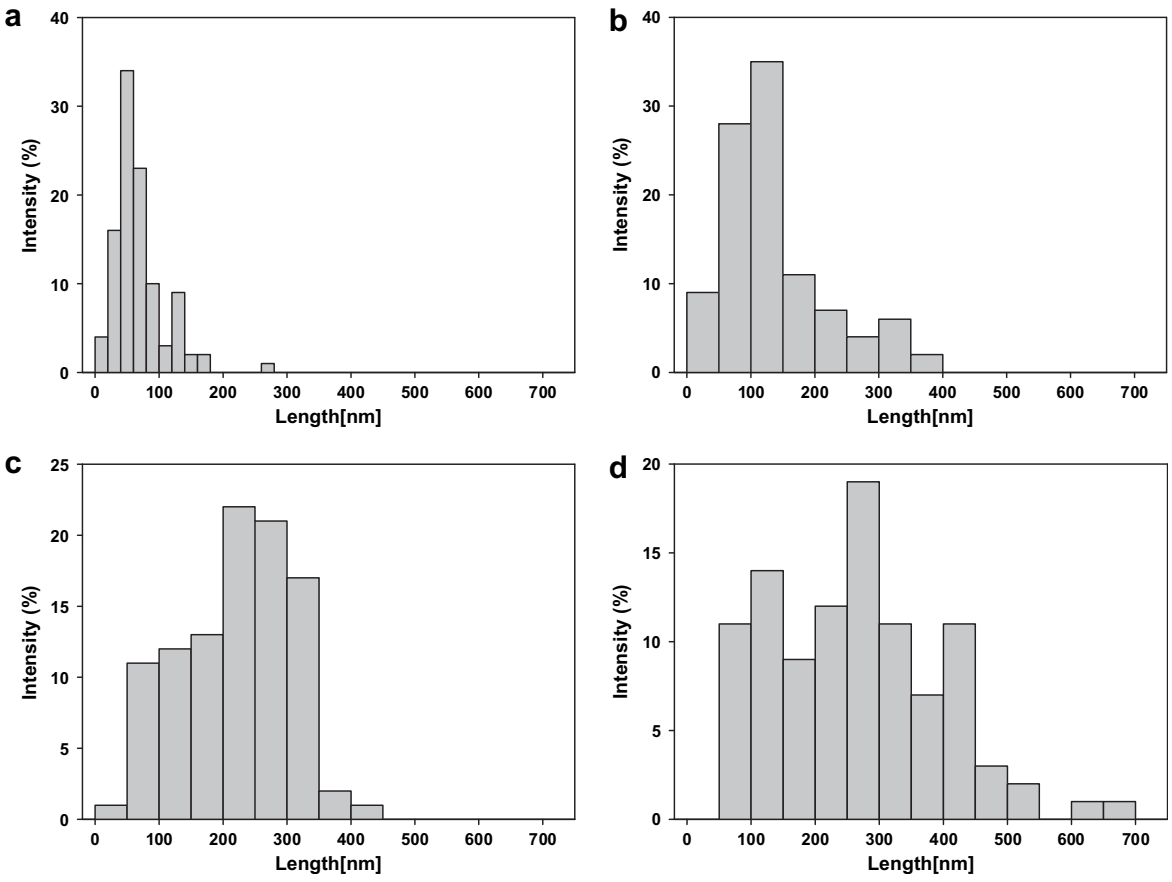

Fig. 7. Histogram of nanotube length distribution for samples prepared in (a) compression molding (b) micro-injection-compression molding (c) conventional injection molding (d) micro-injection molding.

shear rate for this process is relatively the same as that in conventional injection, the nanotube alignment in this case is lower than for conventional injected tensile bars. This is due to the cavity being centrally gated, elongational flow is dominant at the gate (divergent flow) causing the nanotubes to first orient transversely (perpendicular to the main radial flow direction) in the core zone. Near the wall, shear flow dominates and tends to orient the nanotubes in the radial main flow direction. For dog-bone samples, nanotubes are mostly subjected to shear deformation and then are oriented in the flow direction.

Micro-injection-compression molding proceeds in two phases, one with a high shear rate during injection and one with low shear rate during compression. Due to the high level of shear rate, the nanotubes are well aligned at the end of the first step or injection phase. However, during the compression phase, which can be assimilated to a squeeze flow, elongational flow perpendicular to the radial direction can be significant and diminish the effects of the first step (injection) on the nanotube alignment. As a result, a more isotropic structure is formed. Consequently, micro-injection compression molding produces parts with the lower intensity ratios for the Raman *D* and *G* bands.

Finally the lowest level of nanotube alignment is obtained when a circular disk is produced using manual compression molding for which of the radial flow proceeds at extremely low deformation rate.

It is worthy to mention that the highest values of $D_{\prod}/D_{\perp}$ for carbon nanotubes are normally reported for nano or microfibers. In the case of melt spun PC nanofibers this ratio was found to be around 2.1 for PC/MWCNT [10] and around 2.6 for PC/SWCNT nanofibers [17]. Accordingly, the values found in this study for highly aligned nanotubes are somehow close to those related to spun fibers indicating that the alignment due to micro-injection can be very high.

The *D*/*G* ratio is often used as a diagnostic tool for checking the degree of perfection of MWCNTs [32] or the degree of crystallinity in the nanotube structure [13]. A constant value of *D*/*G*, in both parallel and perpendicular geometries, then means that there is no change in the nanotube structure [40]. To check the induced

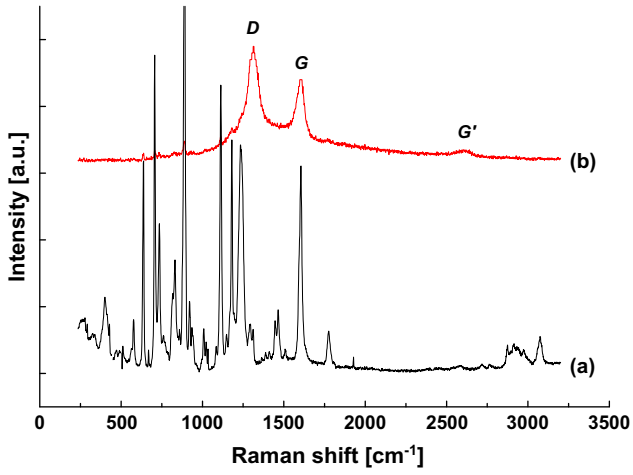

Fig. 8. Raman spectra of neat polycarbonate (a) and PC/5 wt% MWCNT (b).

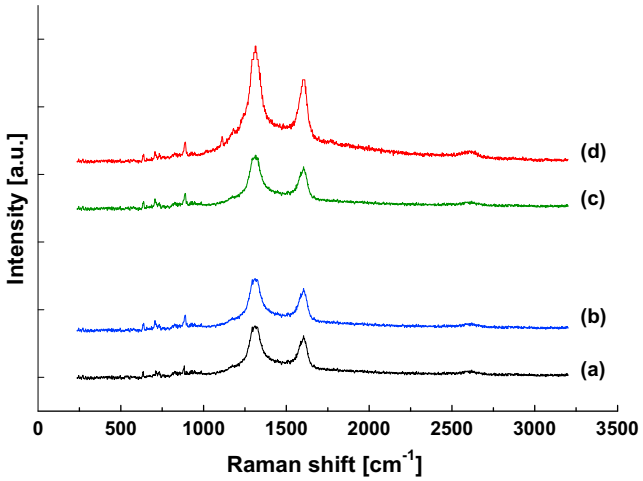

Fig. 9. Raman spectra of PC/5 wt% MWCNT nanocomposites: bottom two; compression molded samples, top two, microinjected samples; (a) and (c) perpendicular, (b) and (d) parallel arrangements.

changes in the crystalline structure of MWCNTs, we used the ratio of $(D/G)_{\prod}/(D/G)_{\perp}$. If the nanotubes do not go through structural changes the D/G values is constant and $(D/G)_{\prod}/(D/G)_{\perp}$ ratio should be equal to 1. As one can deduce from Table 1 this ratio is between 1.03 and 1.11 for all processes indicating that the crystalline structure of individual nanotubes is more or less stable.

4.3. Rheological properties

It is widely accepted that shear flow reduces markedly the particle–particle interactions and leads to a remarkable change of the viscoelastic behavior [41]. The percolation network of nanotubes is therefore quite sensitive to steady shear flow [42]. In order to investigate the effect of shear flow during polymer processing on the PC/MWCNT post-molding viscoelastic properties, SAOS rheological tests were conducted on compression, micro-injection-compression and microinjected molded disk shaped samples at 300 °C, the average barrel temperature used in our processes. Fig. 10 shows the effect of the different processing methods on the complex viscosity of the neat polycarbonate and the nanocomposites containing 5 wt% of MWCNTs. Obviously, for the neat polycarbonate the effect of processing conditions is negligible. However, for the 5 wt% nanocomposite this effect becomes quite large. The complex viscosity decreases by about two orders of magnitude for the sample made by micro-injection molding, the process which features the highest levels of shear rate. Even the lower effective shear rate of micro-injection-compression molding significantly shifts the complex viscosity to lower values. Note that the shear-thinning behavior of the nanocomposites is also affected by the processing method. Fig. 10 reveals that for the 5 wt% nanocomposite the viscosity tends towards a plateau at high frequency. This is more striking for high shear rate processes. A similar trend was observed in our last work when pre-shearing a 3% MWCNT/PC nanocomposite at 300 °C [34]. The drastic reduction in viscosity and change in the shear-thinning behavior shown in Fig. 10 could be explained by the idea that carbon nanotubes tend to behave like macromolecules in solution. Under such high shear rates and shear stresses encountered in micro-injection molding, the nanotubes no longer "stick" together and are subjected to flow induced disentanglement and alignment exhibiting shear-thinning effect just like entangled polymer chains would in high shear flow conditions [43–45].

The rheological percolation threshold is also affected by the processing method. The percolation threshold is often defined as the value of the solid content above which the rheological properties increase in an exponential way. Fig. 11 shows the storage modulus data reported as a function of nanotube content. The percolation threshold can be determined by applying a power-law function to G′ versus nanotube loading according to the following equation [6,12,46–48]:

$$G' = \beta_{c,G}\left(\frac{m - m_{c,G}}{m_{c,G}}\right)^{q} \quad \text{for } m > m_{c,G} \tag{16}$$

where $\beta_{c,G}$ and q are parameters, m is nanotube loading (wt%) and $m_{c,G}$ is the percolation threshold (wt%). The description of the data by Eq. (16) is shown in Fig. 11 to be excellent and the left limit of the dashed line corresponds to the percolation threshold value. The figure clearly shows that the percolation threshold is shifted towards larger nanotube content when the processing is carried out under higher effective shear rates and large stress for the pre-sheared sample in the rheometer.

We also measured the percolation threshold in SAOS after applying a pre-shearing stress corresponding to the maximum allowable value for the CSM rheometer (2400 Pa). [34]. As soon as

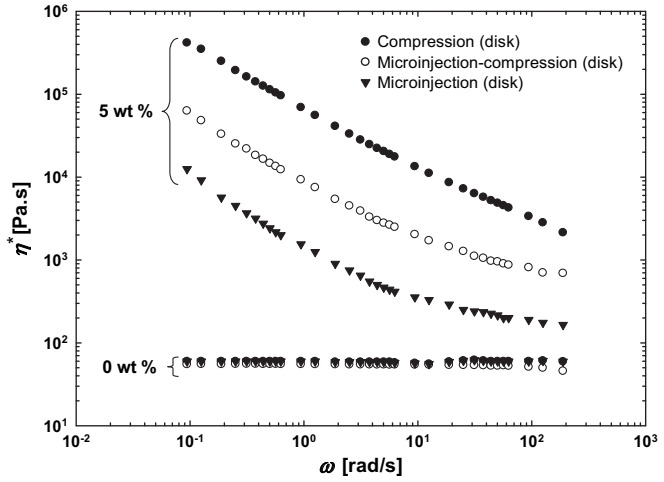

Fig. 10. Complex viscosity at 300 °C of neat polycarbonate and PC/5 wt% MWCNT nanocomposites for different processing methods.

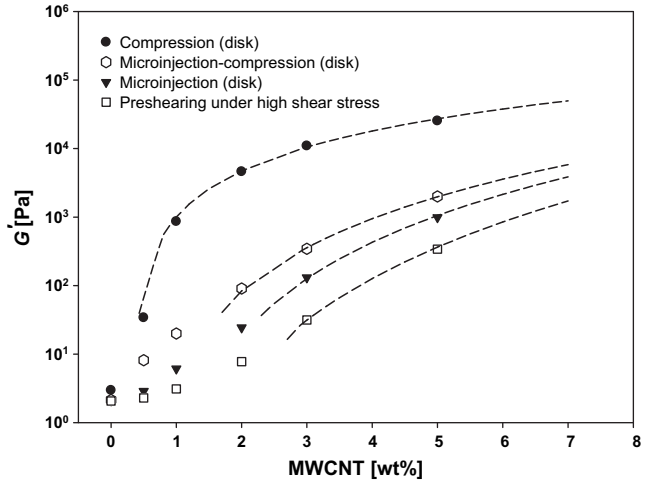

Fig. 11. Effect of processing conditions and pre-shearing at 2400 Pa (without rest time) on G′ data (1 rad/s) at 300 °C.

the pre-shearing step was completed (i.e. the shear viscosity has reached steady-state), SAOS tests were conducted without any rest time. As we expected, the effect of applying a high shear stress is more or less similar to the effect encountered in micro-injection molding. In all cases the percolation threshold increases remarkably when the nanocomposites are subjected to high shear flow. As in the case of microinjected samples, we do not have a perfect or ideal percolated network in the presheared samples even at high nanotube loading as the storage modulus rises less markedly with nanotube concentration above the threshold.

4.4. Electrical conductivity

As the electrical conductivity of nanocomposites is one of the main properties of interest in this work, we investigated the effect of polymer processing on the electrical conductivity of the nanocomposites, particularly prepared by micromolding. Moreover, measurement of the electrical properties may be a useful tool to understand the relationship between the rheological behavior and the nanocomposites microstructure. Fig. 12 presents the effect of nanotube loading on the electrical conductivity of the nanocomposites samples prepared by the same processing methods as previously.

Like the rheological percolation threshold, the electrical percolation threshold can be described by a similar power-law expression [6]:

$$\sigma = \beta_{c,\sigma}\left(\frac{m - m_{c,\sigma}}{m_{c,\sigma}}\right)^{q} \quad \text{for } m > m_{c,\sigma} \tag{17}$$

where $\beta_{c,\sigma}$ and q are parameters, $m_{c,\sigma}$ is the electrical percolation threshold (wt%) and σ the electrical conductivity. Again this power-law expression is found to describe very well the data of Fig. 12 where the left limit of the dashed line corresponds to the percolation threshold value in each case.

For compression molded samples the percolation threshold is found to be about 3 wt% nanotube content as the electrical conductivity rises suddenly by more than 10 decades. Above these concentrations, the conductivity increases slightly to eventually reach a plateau. This is typical of the percolation behavior usually observed for nanocomposites based on conductive fillers, and can be referred to as an ideal percolation behavior. Fig. 12 shows that for samples made by a process involving an injection step, a rather monotonic increase of conductivity with loading is obtained. As stated previously, in injected samples the nanotubes are more or less well aligned in the flow direction depending on the level of shear rate, limiting the likelihood of close proximity and connection. A conductive pathway of nanotubes can then be formed only at high nanotube contents where the aligned nanotubes are close enough to allow for current passage. It is obvious that in such a condition, since there is no percolated network formed in the system anymore, the larger the nanotube loading is the shorter is the distance between the nanotubes and the higher is the conductivity level. Therefore, no sudden jump in electrical conductivity or percolation point is observed in Fig. 12 for the injected samples, but rather a broad range of percolation over which electrical conductivity increases continuously. Micro-injection molding proceeds under extremely high levels of effective shear rate and almost completely aligns the nanotubes in the flow direction. Consequently, the percolation threshold estimated by Eq. (17) has larger values for parts produced by micro-injection. The longitudinal flow in the dog-bone shaped cavity results in the highest value for the percolation threshold, about 9 wt% of nanotube loading.

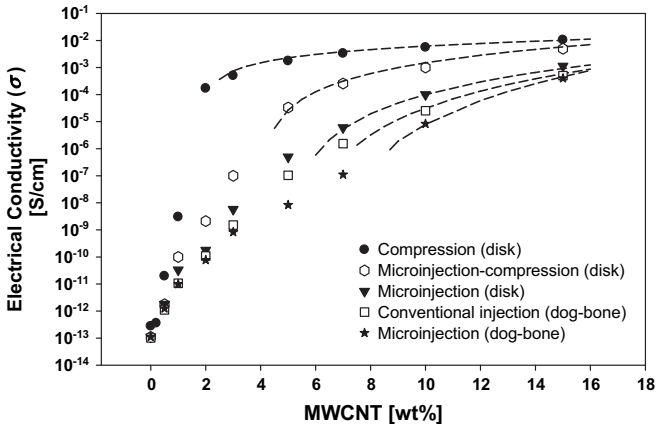

Fig. 12. Effect of polymer processing conditions on the electrical conductivity and electrical percolation threshold of the nanocomposites.

Interestingly, the calculated percolation threshold is highly affected by the mold geometry. As Fig. 12 reveals that for the disk shaped microinjected samples the percolation threshold is lower and the electrical conductivities are about one order of magnitude larger than that of dog-bone shaped samples. The radial (elongational) flow in the disk shape cavity reduces the effect of high shear rate and less nanotube alignment is achieved due to the elongational flow component, which orients the nanotubes transversely to the radial flow direction. This favors the formation of a percolated network. Both compression molding and micro-injection-compression molding of disk shaped samples achieve similar levels of nanotube orientation in the transverse and radial flow directions. As a consequence, the electrical percolation threshold behavior pertaining to both processing methods are closely similar as can be seen from Fig. 12.

4.5. Mechanical properties

The mechanical properties of dog-bone microinjected samples were analyzed and Fig. 13 shows the influence of MWCNT concentration on the stress–strain behavior of microinjected tensile parts. Obviously the neat polycarbonate and the 0.5 wt% nanocomposite specimen show strain a hardening behavior and necking at high elongation. However, the nanocomposites with larger nanotube loadings show no strain hardening and become more brittle as the strain-to-failure decreases with nanotube concentration. All samples, with the exception of the largest concentration nanocomposite, show yielding before plastic flow.

The values for the strength and the elongation at break of the nanocomposites of different nanotube loadings are summarized in Fig. 14. We first observe a slight decrease in strength then an increase with MWCNT loading above 1% weight concentrations probably due to the formation of nanotube network at this level of loading. The effect of nanotube loading on the nanocomposite ultimate strength is not very significant and the overall tendency demonstrates only a modest increase with MWCNT concentration. This is probably due to the poor interaction between nanotubes and polymer chains so that the nanotubes could not achieve their theoretical potential as fillers with extremely high strength. Elongation at break is also strongly affected by nanotube loading, starting to decrease drastically for composites containing up to 1% of nanotubes. Beyond this concentration, ductility decreases at a lower rate until the samples become totally brittle at loadings of about 7–10 wt%. The structural change of the nanocomposite with increasing nanotube content is probably responsible for this phenomenon. Above 1 wt%, the formation of nanotubes aggregates or agglomerates could change the load transfer mechanism of the

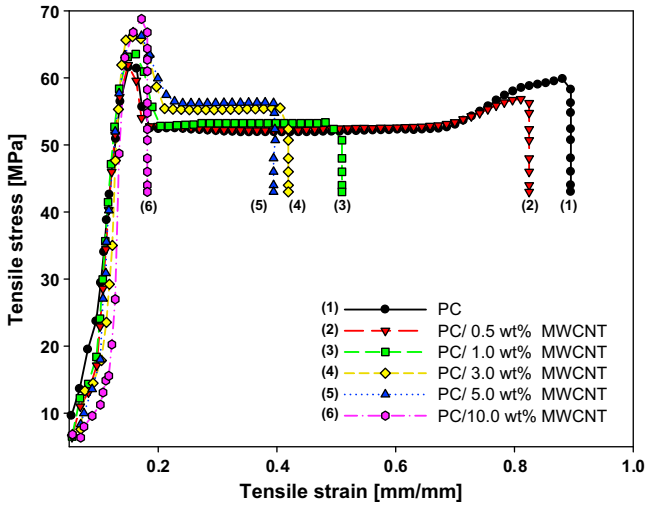

Fig. 13. The effect of MWCNT content on the stress–strain behavior of dog-bone shaped microinjected nanocomposites.

nanocomposites and result in a different trend in the mechanical properties.

The effect of MWCNT loading on the Young modulus of the nanocomposites, obtained from a closer view of the stress–strain curves (Fig. 13), is shown in Fig. 15. The Young modulus increases monotonically with loading and tends towards a plateau for large nanotube levels. The addition of 3 wt% of nanotubes results in a rise of the modulus by about 30%. Again, this is a weak effect of nanotube on the tensile modulus probably due to weak interactions between polymer chains and the filler.

Fig. 15 also shows that the Young modulus is larger when the injection speed is the largest due to higher polymer chain orientation and larger degree of nanotube alignment. Although the effect is not highly significant, it is different from what reported previously in the case of conventional injection molding of polymer/long fiber composites like Kevlar [49]. They found that lower injection speeds create a thicker solidified layer and result in a higher shear flow field at the solid–melt interface. It is also shown that the polymer relaxation prior to solidification in the mold reduces the orientation in conventional injection [50]. Higher as the injection speed increases the solidification time is increased and this results in a more relaxation. Consequently polymer chains are less oriented and fibers are less aligned in flow

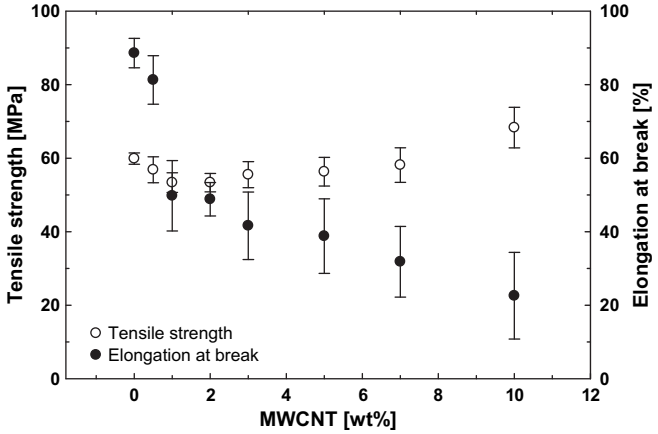

Fig. 14. The effect of MWCNT content on the tensile strength and elongation at break of dog-bone shaped microinjected nanocomposites.

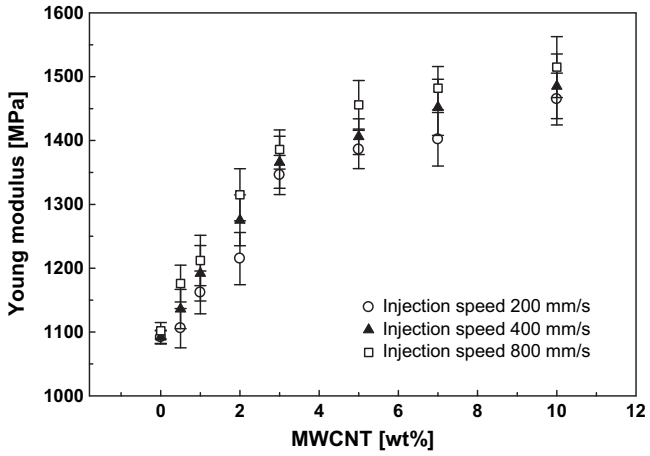

Fig. 15. Effect of micro-injection speed on the Young modulus of the dog-bone shaped nanocomposites of different tube contents.

direction (along the length of the tensile bars). In the case of micro-injection molding, due to very small thickness of the sample, cooling is highly efficient and the cooling time is very short. The whole sample solidifies rapidly and there is not enough time for the polymer chains to relax. Therefore, increasing the injection speed results in a higher orientation since the relaxation process is somehow negligible in this process. It is worthwhile to note that the values obtained for the Young modulus of the microinjected parts, even for the neat polycarbonate, are considerably smaller than the typical values obtained for conventional or standard samples tested under the same test conditions (for the neat polycarbonate this value is about half of the standard values). It is still unclear to us why the microinjected parts have such low tensile modulus [51]. Our rheological measurements revealed that the degradation during this process was insignificant; the viscosity of the neat polycarbonate after processing was found to be similar to that before molding within the experimental error.

5. Discussion

It has been observed that the nanocomposites properties strongly depend on the processing conditions. Such dependency of the percolation threshold of nanotube-based nanocomposites has been established qualitatively in the literature [13,16] where the melt-processed films or fibers showed high electrical conductivity at low draw ratios but below the detection limit at high draw ratios. It seems that by changing the nanotube alignment in the nanocomposites we can control the nanocomposite properties. For instance, using a certain amount of nanotube loading, it would be possible to have conductive or resistive materials only by changing the flow type and the effective shear level. This interesting issue is discussed in this section. It is worthwhile to note that the rheological percolation threshold is considerably smaller than the electrical one for the same processing conditions. This difference can be described in terms of the shorter tube–tube distance required for electrical conductivity as compared to that required to impede polymer mobility, so that more nanotubes are required to reach the electrical percolation threshold. However, in spite of the fact that these percolating networks are due to different phenomena, their structures change in a similar way when they are subjected to a flow field. Clearly, if nanotubes start to be aligned in the flow direction, they interconnect minimally, as their orientations become less random, leading to a remarkable increase in the percolation threshold.

To investigate these aspects in more details, the electrical and rheological percolation thresholds are plotted against the $D_{\prod}/D_{\perp}$ ratio, Raman intensity parallel/perpendicular to the flow direction, in Fig. 16. In the case of the rheological threshold, it was more convenient to use disk shaped samples molded by compression, micro-injection-compression and micro-injection for the post-molding rheological properties measurements. The values of G' and σ obtained for the 5 wt% MWCNT nanocomposites are also shown in the figure. As observed, the percolation threshold is quite low at low $D_{\prod}/D_{\perp}$ ratio, which is an indication that the nanotubes networks are formed at very low concentrations when random orientation ($D_{\prod}/D_{\perp} \sim 1$) prevails.

The percolation thresholds significantly rise with $D_{\prod}/D_{\perp}$ ratio (or nanotube alignment) so that in the highly aligned cases, like in microinjected samples where $D_{\prod}/D_{\perp}$ is around 1.95, the electrical percolation threshold is about 9 wt% of MWCNT, which is quite high. More interestingly G' and σ decrease remarkably with increasing $D_{\prod}/D_{\perp}$ ratio or nanotube alignment. We can therefore conclude that the $D_{\prod}/D_{\perp}$ ratio is closely related to specific nanocomposites properties such as G' and σ. In addition, the power-law type equations (Eqs. 16 and17) characterize well the post-percolation behavior and provide reasonably accurate values of the percolation thresholds. From the previous results of Figs. 11 and 12, we observe that processing conditions that yield a nearly perfect percolation behavior tend to display a plateau immediately above the percolation threshold, indicating that further addition of nanotubes could not notably increase the related property of the nanocomposites. This is especially true for the compression molding parts where the shear stresses and shear rates are the lowest. In this situation, it is found that the best fit is achieved when the parameter q is $\sim$1. Deviation from this value is indicative of an absence of a plateau or a perfect percolation behavior. In this case we see a broad range of percolation and the related properties keep increasing after percolation. This is more applicable to the electrical percolation rather than the rheological percolation behavior, since in the former case complete tube–tube contacts are required to have a conductive network. The q values determined by fitting the respective power-law equations are shown in Fig. 16 versus the $D_{\prod}/D_{\perp}$ ratio. Of special interest is the significant increase in q as the nanotube alignment increases indicating that the percolation of highly aligned nanotubes is hardly possible.

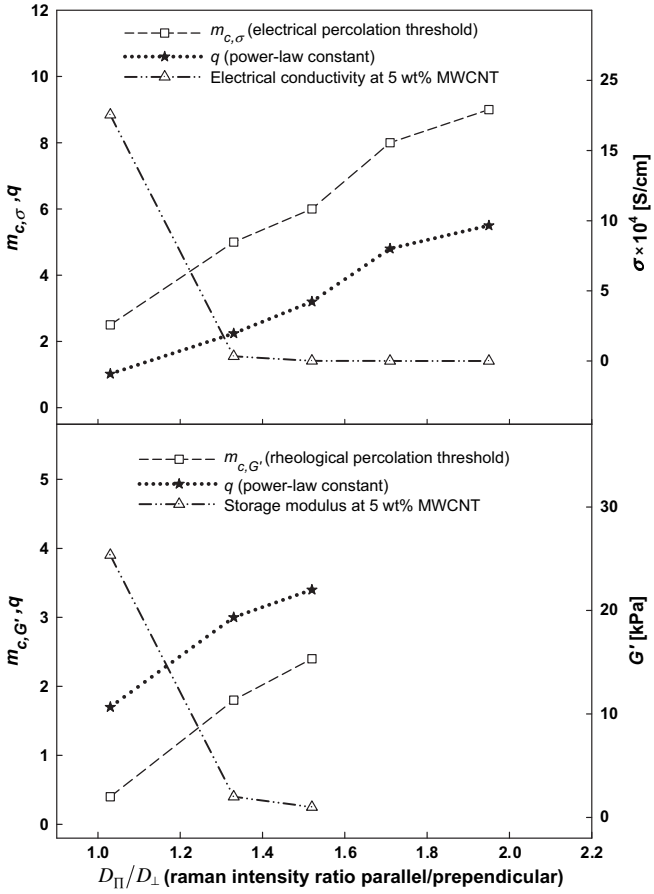

Fig. 16. Effect of nanotube alignment on the rheological and electrical percolation thresholds of the nanocomposites, on the storage modulus and electrical conductivity of PC/5 wt% MWCNT nanocomposites and on the parameter q. $D_{\prod}/D_{\perp}$ values are taken from Table 1.

6. Conclusions

In this work we have examined the effects of polymer processing conditions on the nanotube alignment and PC/MWCNT nanocomposites properties. A masterbatch was diluted to prepare nanocomposites samples at various concentrations and the nanocomposites were then subjected to different flow conditions in a controlled manner employing a variety of polymer processing methods. The morphological analysis, using SEM, TEM and AFM, showed that the nanotubes were randomly oriented in the plane of the compression molded samples, which were subjected to the lowest shear value, while they were well aligned in the longitudinal flow direction in the microinjected dog-bone samples, which featured very high shear values. Raman spectroscopy results indicate that the lowest values of $D_{\prod}/D_{\perp}$ and $G_{\prod}/G_{\perp}$ ratios were obtained for the compression molded samples while the highest values were related to the microinjected dog-bone samples. Interestingly, the nanotube alignment strongly affected the rheological properties and the electrical conductivity of the nanocomposites. The percolation thresholds rose significantly in both cases with increasing orientation level. Further analysis showed that for a given nanotube loading, the nanocomposite electrical conductivity level could be controlled by controlling the nanotube alignment. Moreover, by fitting a power-law equation to the storage modulus and electrical conductivity data we determined reasonably accurate values of percolation thresholds as well as the post-percolation behavior of the nanocomposites. The parameter, q, was found to be a very good parameter to investigate the percolation behavior of nanotube networks. It was found to increase with nanotube alignment, indicating that for highly sheared samples there is no perfect percolation behavior or ideal nanotube network. In these cases broad ranges of percolation were observed. The mechanical properties of the nanocomposites were also found to be sensitive to processing, albeit somehow improved by increasing the shear level.

Acknowledgements

Financial support from NSERC (Natural Science and Engineering Research Council of Canada) is gratefully acknowledged. We are also thankful to Ms. Weawkamol Leelapornpisit for her great help in the morphological studies.

References

[1] Meyyappan M. Carbon nanotubes: science and applications. Boca Raton: CRC Press; 2005.
[2] Wu D, Liang W, Yurong S, Ming Z. Polym Sci B 2007;45(23):3137–47.
[3] Abdel-Goad M, Potschke P. J Non-Newton Fluid Mech 2005;128(1):2–6.
[4] Meincke O, Kaempfer D, Weickmann H, Friedrich C, Vathauer M, Warth H. Polymer 2004;45(3):739–48.

[5] Moniruzzaman M, Winey KI. Macromolecules 2006;39(16):5194–205.
[6] Hu G, Zhao C, Zhang S, Yang M, Wang Z. Polymer 2006;47(1):480–8.
[7] Sung YT, Han MS, Song KH, Jung JW, Lee HS, Kum CK, et al. Polymer 2006;47(12):4434–9.
[8] Shi X, Hudson JL, Spicer PP, Tour JM, Krishnamoorti R, Mikos AG. Nanotechnology 2005;16(7):531–8.
[9] Kharchenko SB, Migler KB, Douglas JF, Obrzut J, Grulke EA. ANTEC; 2004. p. 1877–81.
[10] Potschke P, Fornes TD, Paul DR. Polymer 2002;43(11):3247–55.
[11] Fangming D, Fischer JE, Winey KI. Phys Rev B 2005;72(12):121404–11.
[12] Du F, Scogna RC, Zhou W, Brand S, Fischer JE, Winey KI. Macromolecules 2004;37(24):9048–55.
[13] Pötschke P, Brünig H, Janke A, Fischer D, Jehnichen D. Polymer 2005;46(23):10355–63.
[14] Kharchenko SB, Douglas JF, Obrzut J, Grulke EA, Migler KB. Nat Mater 2004;3(8):564–8.
[15] García Gutiérrez MC, Nogales A, Rueda DR, Domingo C, García-Ramos JV, Broza G, et al. Polymer 2006;47(1):341–5.
[16] Haggenmueller R, Gommans HH, Rinzler AG, Fischer JE, Winey KI. Chem Phys Lett 2000;330(3–4):219–25.
[17] Fornes TD, Baur JW, Sabba Y, Thomas EL. Polymer 2006;47(5):1704–14.
[18] Chae HG, Minus ML, Kumar S. Polymer 2006;47(10):3494–504.
[19] Sung JH, Kim HS, Jin H-J, Choi HJ, Chin I-J. Macromolecules 2004;37(26):9899–902.
[20] Liu LQ, Tasis D, Prato M, Wagner HD. Adv Mater 2007;19(9):1228–33.
[21] Potschke P, Bhattacharyya AR, Janke A. Carbon 2004;42:965–9.
[22] Pham GT, Park YB, Wang S, Liang Z, Wang B, Zhang C, et al. Nanotechnology 2008;19(32):325705.
[23] Ding W, Eitan A, Fisher FT, Chen X, Dikin DA, Andrews R, et al. Nano Lett 2003;3(11):1593–7.
[24] Singh S, Pei Y, Miller R, Sundararajan PR. Adv Funct Mater 2003;13(11):868–72.
[25] Pötschke P, Abdel-Goad M, Alig I, Dudkin S, Lellinger D. Polymer 2004;45(26):8863–70.
[26] Jin L, Bower C, Zhou O. Appl Phys Lett 1998;73(9):1197–9.
[27] Zhao Q, Wagner HD. Philos Transact A Math Phys Eng Sci 2004;362(1824):2407–24.
[28] Litchfield DW, Baird DG. Polymer 2008;49(23):5027–36.
[29] Jehng JM, Tung WC, Kuo CH. J Porous Mater 2008;15(1):43–51.
[30] Lee SN, Stolarski V, Letton A, Laane J. J Mol Struct 2000;521(1–3):19–24.
[31] Jorio A, Dresselhaus G, Dresselhaus MS. In: illustrated, editor. Carbon nanotubes: advanced topics in the synthesis, structure, properties and applications. Springer; 2008.
[32] Bulusheva LG, Okotrub AV, Kinloch IA, Asanov IP, Kurenya AG, Kudashov AG, et al. Phys Status Solidi (B) 2008;245(10):1971–4.
[33] Rao AM, Jorio A, Pimenta MA, Dantas MSS, Saito R, Dresselhaus G, et al. Phys Rev Lett 2000;84(8):1820–3.
[34] Abbasi S, Carreau PJ, Derdouri A, Moan M. Rheologica Acta 2009;48(9):943–59.
[35] Bird RB, Stewart WE, Lightfoot EN. Transport phenomena. 2nd ed. John Wiley & Sons; 2007.
[36] Bird RB, Armstrong C, Hassager O. Dyn Polym Liquids. 2nd ed., vol. 1. John Wiley & Sons; 1987.
[37] Baird DG, Collias DI. Polymer processing principle and design. John Wiley & Sons; 1998.
[38] Laurencena BR, Williams MC. J Rheol 1974;18(3):331–55.
[39] Bliznyuk VN, Singamaneni S, Sanford RL, Chiappetta D, Crooker B, Shibaev PV. Polymer 2006;47(11):3915–21.
[40] Endo M, Kim YA, Fukai Y, Hayashi T, Terrones M, Terrones H, et al. Appl Phys Lett 2001;79(10):1531–3.
[41] Fan Z, Advani SG. J Rheol 2007;51(4):585–604.
[42] Defeng W, Liang W, Ming Z, Yalan Z. J Polym Sci B 2007;45(16):2239–51.
[43] Shafer MSP, Windle AH. Macromolecules 1999;32(20):6864–6.
[44] Green MJ, Behabtu N, Pasquali M, Adams WW. Adams Polymer 2009;50(21):4979–97.
[45] Hobbie EK, Fry DJ. Phys Rev Lett; 2006:97. id. 036101.
[46] Xiao KQ, Zhang LC, Zarudi I. Compos Sci Technol 2007;67(2):177–82.
[47] Zhang Q, Rastogi S, Chen D, Lippits D, Lemstra PJ. Carbon 2006;44(4):778–85.
[48] Thostenson ET, Li C, Chou TW. Compos Sci Technol 2005;65(3–4):491–516.
[49] Yu Z, Ait-Kadi A, Brisson J. Polymer 1994;35(7):1409–18.
[50] Tadmor ZJ. Appl Polym Sci 1974;18:1753–72.
[51] Chu J, Kamal MR, Derdouri A, Hrymak A. ANTEC; 2008. p. 2468–72.